

Manganese oxidation induced by water table fluctuations in a sand column.

Claire E. Farnsworth,^{1,2} Andreas Voegelin,² Janet G. Hering^{2,3,4 *}

¹Division of Engineering and Applied Science, California Institute of Technology,

Pasadena, CA 91125, ²Eawag, Swiss Federal Institute of Aquatic Science &

Technology, Dübendorf, Switzerland, CH-8600, ³Institute for Biogeochemistry and Pollutant

Dynamics, ETH, Zurich, Switzerland, ⁴École Polytechnique Fédérale de Lausanne, School of

Architecture Civil & Environmental Engineering, Lausanne, Switzerland

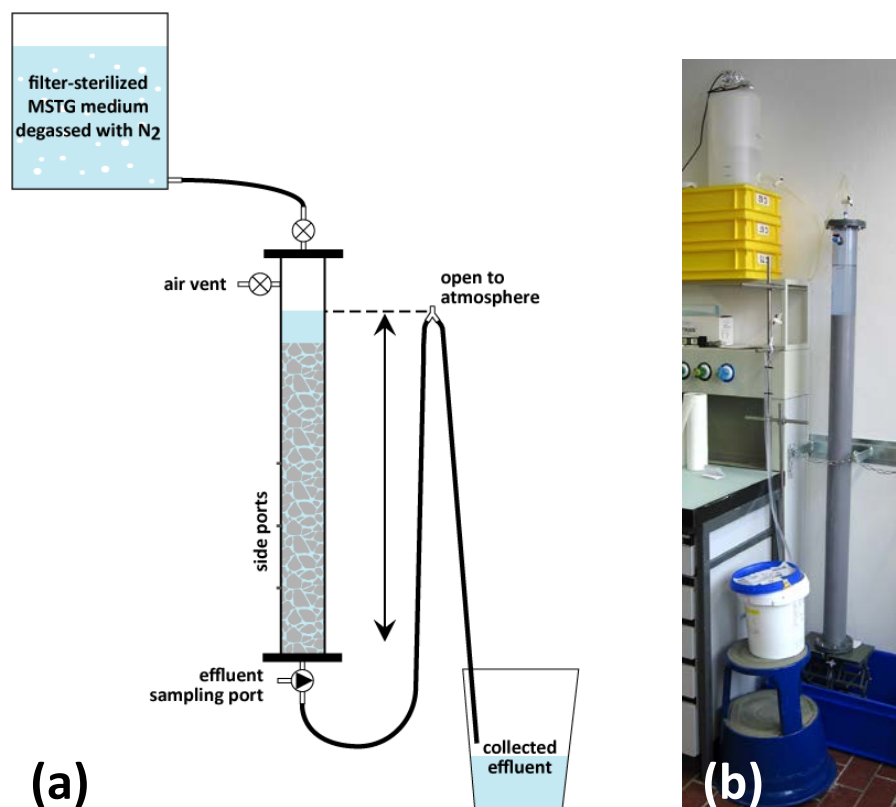
Corresponding author: Eawag, Überlandstrasse 133, CH-8600, Dübendorf, Switzerland

phone +41 (0)58 765 50 01, e-mail: janet.hering@eawag.ch

Supporting Information

Contents: 12 pages, including 6 figures and 3 tables

I.	Figure S1: Schematic of Column Setup	S2
II.	Oxidation Assays at the End of the Column Experiment	S2
	Table S1: Results of Oxidation Assays	S2
III.	Figure S2: Filtered Relative Effluent Concentrations of Br	S4
IV.	XAS Analysis of Sample from the Top of the Sand Column	S5
	Figure S3: XANES and EXAFS spectra of Mn at the top of the sand column	S5
	Table S2: Linear Combination Fit Results for Mn XANES and EXAFS Spectra...	S6
V.	Figure S4: XRF Profile of P along the Column at the End of the Experiment.....	S7
VI.	Reduction Assays	S7
	Table S3: Pseudo-First-Order Rate Coefficients for Mn Oxide Reduction and	
	OD ₆₀₀ during and after the Experiment	S8
	Figure S5: Mass Balance for Unreacted Gels and Batches at the End of the	
	Reduction Assays	S9
VII.	Figure S6: Effluent pH Measured Directly at the Base of the Column.....	S10
VIII.	Details of Abiotic Mn Oxidation Calculations	S10
IX.	References.....	S12



I. **Figure S1.** Schematic (not to scale, a) and photo (b) of the column set up.

II. Oxidation Assays at the End of the Column Experiment

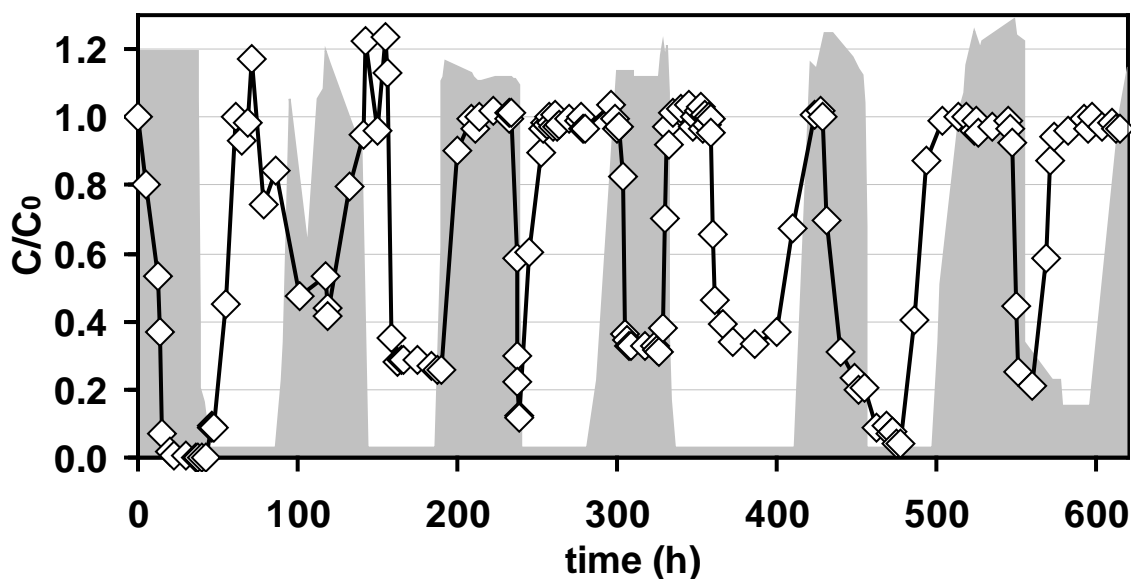
Table S1. Results of oxidation assays at the end of the column experiment.

sample #		OD ₆₀₀ t = 34 h	% Mn(II)	% Mn oxide
1	fresh MSTG, no cells	0.0529	100	0
2	fresh +plate, -Zn	0.1948	1	99
3	fresh +effluent, -Zn	0.1948	1	99
4	fresh +effluent, +Zn	0.3083	100	0
5	influent (+Zn)	0.3532	79	21

The first four batches used freshly prepared and filter-sterilized MSTG medium: (1) without inoculation, (2) inoculated from a plated GB-1 cell culture, and (3) inoculated with the effluent at the end of the column experiment. One effluent-inoculated batch (4) also contained 15 μM ZnCl_2 . In addition, one batch used the column influent solution (5), which contained 15 μM ZnCl_2 , collected at the end of the column experiment without deliberate inoculation; since that

solution should have been sterile, some contamination of the influent with cells able to travel upward along the column walls and through the 0.45 μm filter was suspected.

Lack of growth and oxidation in the fresh MSTG without cells (sample 1) confirms that the MSTG preparation was sterile. Remarkably, the OD_{600} and % oxidation were identical for the Zn-free batches inoculated with column effluent (3a) and directly from the refrigerated LB agar plate (2). Although no replicate assays were performed, this suggests strong similarity between the plated culture and the active culture in the column. The addition of Zn to a batch inoculated with column effluent (3b) resulted in complete inhibition of Mn oxidation, despite a slight growth enhancement. Intriguingly, the cells in the influent that included Zn (4) were able to grow even more and oxidized a fraction of the total Mn (N_2 degassing inhibited cell growth in the influent during the column experiment). This suggests that the pure culture eventually adjusted somewhat to the presence of Zn, or that a mixed culture developed inside the influent reservoir. On the other hand, this batch did not contain visible Mn oxides (+Zn batches had a greenish hue), so it is perhaps more likely that the nonzero Mn oxide fraction in this batch is an artifact of the extraction technique. Even if the column contained a mixed culture, the oxidation of significant amounts of Mn(II) during water table fluctuations does not detract from the end result of the paper.



III. Figure S2. Filtered relative effluent concentrations of Br (\diamond , $C_0 = 10 \mu\text{M}$). For reference, the water level in the column is shown in the shaded profile (note the vertical scale is different than Figure 1). Variation in Br derives from concentration differences in alternate batches of influent solution (“pulsed” inlet concentration). Up to 150 h, preferential flow paths and leaks through the column’s side ports resulted in non-ideal flow behavior. Between concentration pulses, C/C_0 does not always approach 0 because 5-l batches of Br-free MSTG were added to the residual Br-containing MSTG in the influent reservoir, which was always > 0.5 l due to reservoir geometry.

IV. XAS Analysis of Sample from the Top of the Sand Column

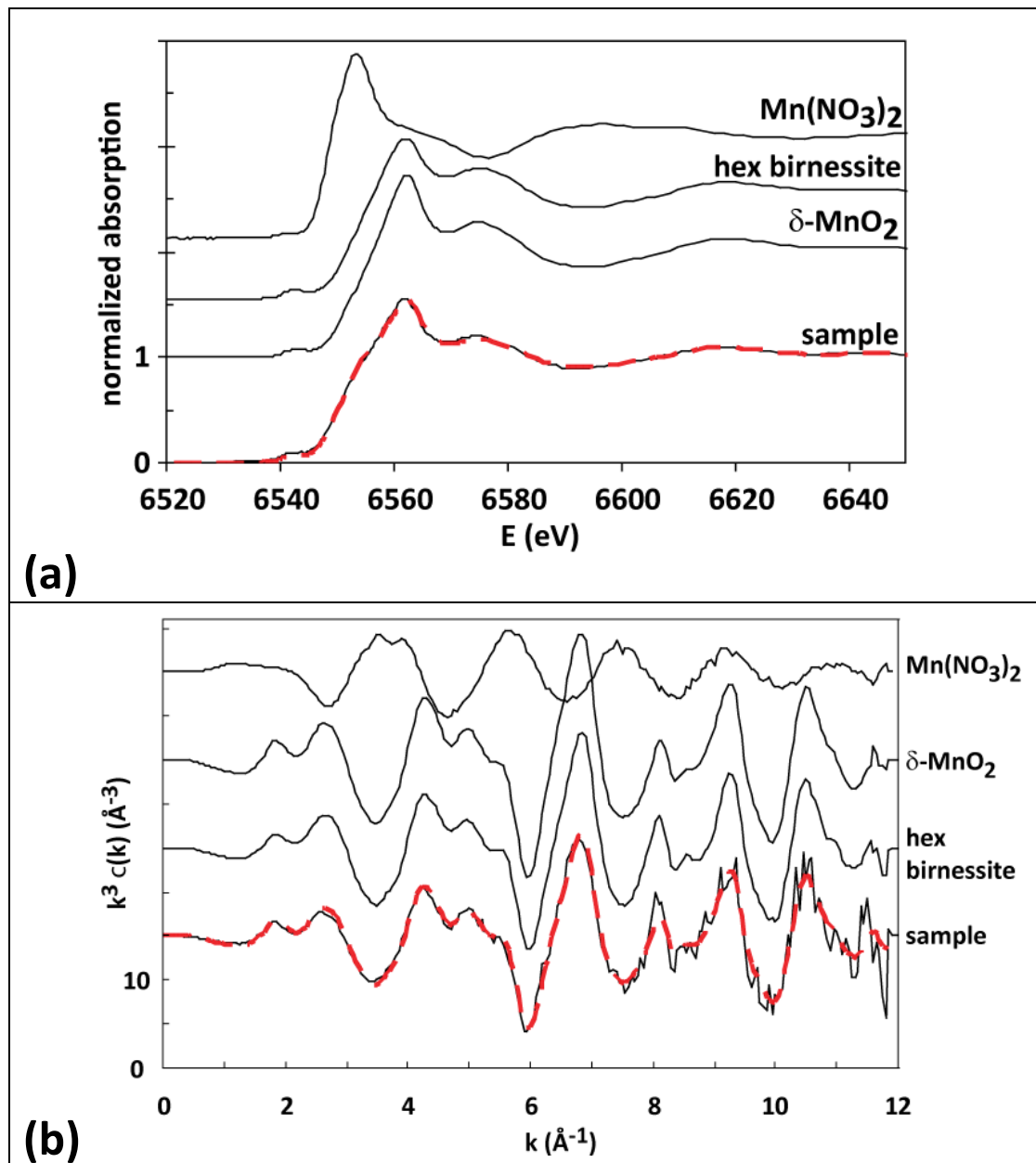


Figure S3: (a) XANES and (b) EXAFS spectra of Mn at the top of the sand column, compared to linear combination fit (LCF) spectra based on reference spectra for aqueous Mn^{2+} , $\delta\text{-MnO}_2$,¹ and hexagonal birnessite.¹ LCF parameters are provided in Table S2.

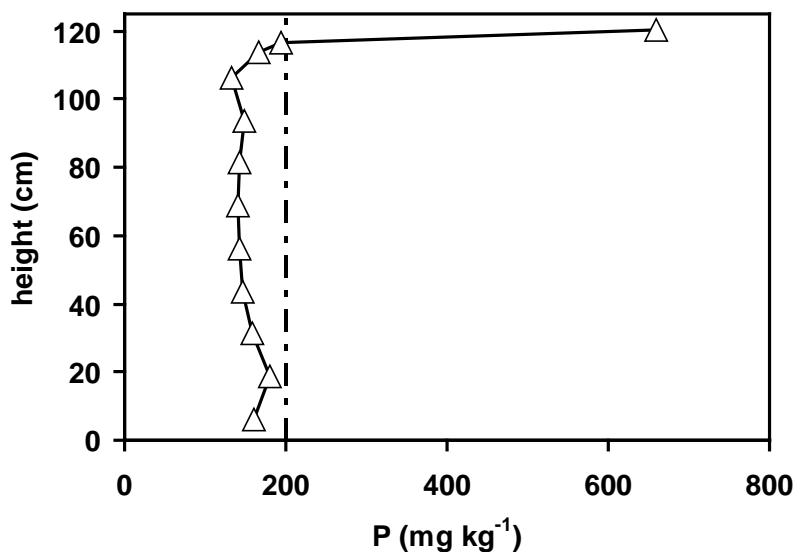
Comparison of the sample spectrum to the spectra of δ -MnO₂ (Mn oxidation state 3.8²) and aqueous Mn²⁺ clearly indicates the presence of some Mn(II) in the sample spectrum. This Mn(II) fraction likely accounts for Mn²⁺ adsorbed to or inside bacteria, or sorbed to the Mn-precipitate or sand. Based on the LCF results for the XANES region (considered more sensitive and reliable than the EXAFS region to quantify the Mn(II) fraction), this Mn(II) fraction was estimated to account for about 20% of the total Mn in the sand sample. Regarding the type of Mn oxide, the features in the EXAFS at 8 and 9.3 Å⁻¹ were characteristic for the phyllophanates δ -MnO₂ and hexagonal birnessite but clearly distinct from the EXAFS of triclinic birnessite or the tectomanganate todorokite.¹ This was confirmed by LCF analysis, which showed that the sample EXAFS spectrum could be reasonably reproduced by a combination of δ -MnO₂ and hexagonal birnessite.

Table S2: Linear Combination Fit Results for Mn XANES and EXAFS Spectra at the top of the sand column.

	δ -MnO ₂	hexagonal birnessite	aqueous Mn ²⁺	sum	NSSR ^a
XANES	0.53 (0.04) ^b	0.28 (0.04)	0.20 (0.00)	1.01	4.6×10 ⁻⁴
EXAFS	0.53 (0.13)	0.30 (0.14)	0.07 (0.00)	0.91	4.5×10 ⁻²

^anormalized sum of squared residuals = $\sum(\text{data}_i - \text{fit}_i)^2 / \sum \text{data}_i^2$

^bvalues in parentheses indicate fit uncertainty



V. Figure S4. XRF profile of P along the column at the end of the experiment. Dashed line indicates the background of unused sand. Other measured elements had no significant trend with height (not shown). Of note, the Fe concentration was below detection (5 mg kg^{-1}) in all samples.

VI. Reduction Assays

To determine whether MSTG media and *P. putida* GB-1 were able to reduce Mn oxides, 3 batch experiments with hydrous Mn oxide-doped gels³ ($2 \text{ mm} \times 5 \text{ mm} \times 2 \text{ cm}$ in dimension) were conducted, with 3 replicates each. Because the microbial cells are physically separated from the Mn oxide inside the gels (which float freely in solution), the assay could separately account for Mn reduction inside the gel and Mn re-oxidation in solution, outside the gel. 25 ml MSTG medium was added to sterile 50-ml centrifuge tubes. Two of the batches were inoculated with 100 ml GB-1 from a dense ($\text{OD}_{600} \sim 1.0$) LB culture. At $t=0$, 3 hydrous Mn oxide-doped gels each were added to the non-inoculated batch (“blank”) and one of the inoculated batches (“exponential”). All three batches were added to a rotary shaker at 180 rpm at room temperature. After the onset of stationary phase, at $t=15 \text{ h}$, 3 hydrous Mn oxide-doped gels were added to the

second inoculated batch (“stationary”). At t=64 h, the gels were harvested and the solutions sampled. In both the gels and the solutions, the remaining Mn was extracted first with 0.05 M $\text{Cu}(\text{NO}_3)_2$ in 0.05 M $\text{Ca}(\text{NO}_3)_2$, then with 0.5% hydroxylamine-HCl to give an approximate measure of Mn(II) and total Mn.⁴ Extracted solutions were filtered (0.2 μm nitrocellulose, Whatman), diluted, and analyzed with ICP-MS (Agilent 7500cx). Solutions were also monitored for OD_{600} at 15 and 64 h. Gel Mn data were analyzed using the MATLAB code provided in the literature⁵ to estimate the pseudo-first-order rate constants for Mn oxide reduction.

Table S3. Pseudo-first-order rate coefficients for Mn oxide reduction and OD_{600} during and after the experiment (averages of 3 replicate batches).

	$k' \text{ (h}^{-1}\text{)}$	$\text{OD}_{600} \text{ t} = 15 \text{ h}$	$\text{OD}_{600} \text{ t} = 64 \text{ h}$
blank: MSTG only	0.0030 ± 0.0015	0.0531	0.0396
exponential: MSTG + <i>P. putida</i> GB-1 ^a	0.0047 ± 0.0012	0.4328	0.2037
stationary: MSTG + <i>P. putida</i> GB-1 ^b	0.0041 ± 0.0022	0.4441	0.2125

^a Mn-doped gels were added at the beginning of exponential phase.

^b Mn-doped gels were added at the beginning of stationary phase.

The rates for the two types of *P. putida* batches were not significantly different. Relatively large standard deviations for k' (up to 50%) reflect the low amounts of Mn lost from the gels relative to the variation between individual gels. OD_{600} for the blank likely decreased due to colloidal components diffusing into the gels. The difference in OD_{600} at 15 h for exponential and stationary batches suggests a small inhibition of cell growth by the polyacrylamide gels doped with hydrous Mn oxide.

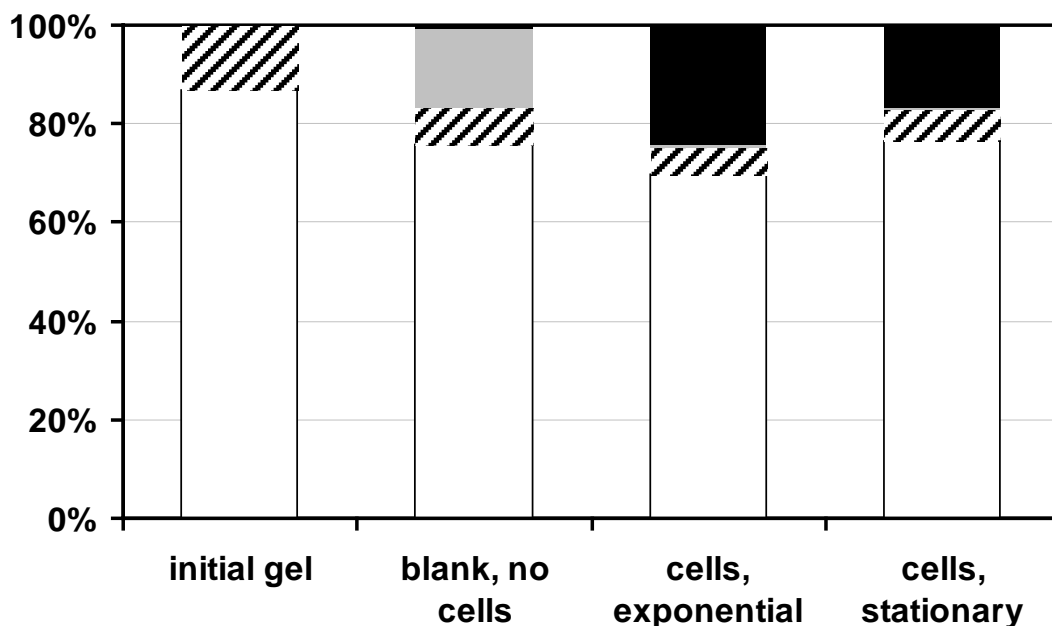
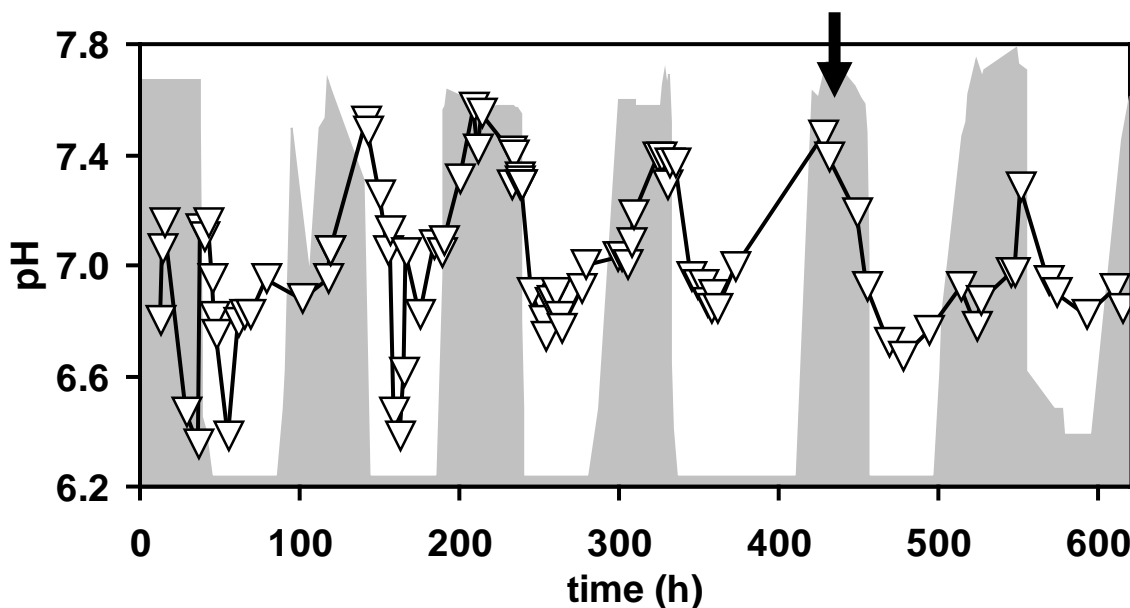


Figure S5. Mass balance for unreacted gels (“initial gel”) and batches at the end of the reduction assays (three replicates each), given as % of total mol Mn per batch. The white bar represents Mn oxide remaining in the gel, the striped bar represents Mn(II) remaining in the gel, the grey bar represents Mn(II) in solution, and the black bar represents Mn oxide in solution. Mn(II) was extracted with 0.05 M $\text{Cu}(\text{NO}_3)_2$ in 0.05 M $\text{Ca}(\text{NO}_3)_2$, while Mn oxide was calculated from the hydroxylamine-HCl-extracted total Mn minus the Mn(II). Total mass balance for each set of batches was closed within 4%. In the absence of cells, MSTG medium oxidized 4% of the solution-phase Mn (0.7% of the total Mn) in 64 h, which is negligible.



VII. Figure S6. Effluent pH (∇ , influent pH = 7.5) measured directly at the base of the column. The arrow denotes the addition of 15 μM Zn to the influent. For reference, the water level in the column is shown in the shaded profile (note the vertical scale is different than Fig. 1). Low values in pH (< 6.6) before 60 h may indicate washout of residual amounts of Nanopure water (pH 5.5) trapped in the pore spaces.

VIII. Details of Abiotic Mn Oxidation Rate Calculations

Abiotic Mn oxidation rate expressions are well-established in the literature. Homogeneous Mn oxidation rate has been expressed⁶:

$$-\frac{d[\text{Mn}^{2+}]}{dt} = k_1[\text{O}_2][\text{OH}^-]^2[\text{Mn}^{2+}] = k[\text{Mn}^{2+}] \quad (1)$$

where k_1 is approximately $2 \times 10^{12} \text{ M}^{-3} \text{ d}^{-1}$, and k represents the pseudo-first-order rate constant.

Heterogeneous Mn oxidation in this system is dependent on two different surfaces for catalysis: Mn oxides, here represented as MnO_2 , and quartz sand, here represented as SiO_2 . Mn adsorption to both surfaces has a reported⁷ half-life of 5 min, so oxidation is assumed to be the only relevant

step in the oxidation rate. Surface catalysis by Mn oxides was studied using hydrous Mn oxide (δ -MnO₂)⁸, which is a high-surface-area analog of natural biogenic Mn oxides². Its ability to catalyze Mn oxidation has been expressed⁶:

$$-\frac{d[\text{Mn}^{2+}]}{dt} = k_{\text{Mn}}[\text{O}_2][\text{OH}^-]^2[\text{MnO}_2][\text{Mn}^{2+}] = k_s[\text{MnO}_2][\text{Mn}^{2+}] \quad (2)$$

where k_{Mn} is approximately $5 \times 10^{12} \text{ M}^{-4} \text{ d}^{-1}$. The surface area and reactivity of δ -MnO₂ are assumed to be approximately equivalent to that of the Mn oxides in the column. Surface catalysis by SiO₂ was studied with nanoparticulate silica⁷, a significantly different material than quartz sand. The rate expression for SiO₂-catalyzed Mn oxidation is:

$$-\frac{d[\text{Mn}^{2+}]}{dt} = k''a\{(>\text{SO})_2\text{Mn}\}p\text{O}_2 = k''a^* \beta_2^s \{\text{SOH}\}[\text{Mn}^{2+}][\text{H}^+]^{-2} p\text{O}_2 \quad (3)$$

where k'' is $0.01 \text{ min}^{-1} \text{ atm}^{-1}$, a is the mass loading (g l^{-1}), β_2^s is $10^{-13.9} \text{ M}$, and $\{\text{SOH}\}$ is $0.0015 \text{ mol g}^{-1}$, following Davies and Morgan⁷. The surface area of nanoparticulate silica ($182 \text{ m}^2 \text{ g}^{-1}$) is orders of magnitude larger than that of the quartz sand, which was estimated to be $9.4 \times 10^{-3} \text{ m}^2 \text{ g}^{-1}$ based on spherical particles with a diameter of 0.24 mm and a density of 2.65 g cm^{-3} (the surface area was too low to be measured by BET). The reactive surface sites and bidentate surface complexes are assumed to be the same for the two solids, and the reactivity is assumed to be proportional to the surface area. Thus, the rate constant k'' was scaled to the surface area of the quartz sand in the column.

To calculate the abiotic oxidation rates at the conditions inside the column, dissolved oxygen in equilibrium with air (or in the case of equation (3), $p\text{O}_2$ was 0.21 atm) and pH 7 were assumed. The maximum effluent dissolved oxygen was only 42% saturation (Figure 2) and influent DO was always <10%, so the calculated rates are faster than expected for the column's

conditions. Although pH fluctuated between 6.35 and 7.55 (Figure S6), the average was 7.01. The molar concentration of MnO₂ in equation (2) was estimated with the average XRF concentration across the column at the end of the experiment (20.5 mg kg⁻¹), the mass of Mn, and the mass of sand (~10 kg) in the column volume (~ 6 l). The mass of sand per liter was also used as “a” in equation (3). Finally, the influent [Mn²⁺] of 100 μM was used in equations 1-3 and the units converted to μM h⁻¹.

IX. References

1. Webb, S. M.; Tebo, B. M.; Bargar, J. R., Structural characterization of biogenic Mn oxides produced in seawater by the marine *Bacillus* sp. strain SG-1. *Am. Mineral.* **2005**, *90*, (8-9), 1342-1357.
2. Villalobos, M.; Toner, B.; Bargar, J.; Sposito, G., Characterization of the manganese oxide produced by *Pseudomonas putida* strain MnB1. *Geochim. Cosmochim. Ac.* **2003**, *67*, (14), 2649-2662.
3. Farnsworth, C. E.; Hering, J. G., Hydrous Manganese Oxide Doped Gel Probe Sampler for Measuring In Situ Reductive Dissolution Rates. 1. Laboratory Development. *Environ. Sci. Technol.* **2009**, *44*, (1), 34-40.
4. Warden, B. T.; Reisenauer, H. M., Fractionation of Soil Manganese Forms Important to Plant Availability. *Soil Sci. Soc. Am. J.* **1991**, *55*, (2), 345-349.
5. Farnsworth, C. E.; Griffis, S. D.; Wildman, J. R. A.; Hering, J. G., Hydrous Manganese Oxide Doped Gel Probe Sampler for Measuring In Situ Reductive Dissolution Rates. 2. Field Deployment. *Environ. Sci. Technol.* **2009**, *44*, (1), 41-46.
6. Morgan, J. J., Manganese in natural waters and earth's crust: its availability to organisms. In *Manganese and its role in biological processes*, Sigel, A. S., Ed. Marcel Dekker, Inc.: New York, 2000.
7. Davies, S. H. R.; Morgan, J. J., Manganese(II) oxidation kinetics on metal oxide surfaces. *J. Colloid Interf. Sci.* **1989**, *129*, (1), 63-77.
8. Morgan, J. J.; Stumm, W., Colloid-chemical properties of manganese dioxide. *J. Colloid Sci.* **1964**, *19*, (4), 347-359.